Submitted to the International Europhysics Conference on High Energy Physics,
HEP97, Jerusalem, Israel, August 1997

Dijet Rates in Deep–Inelastic Scattering at HERA

H1 Collaboration

Abstract

Differential dijet rates have been measured in deep inelastic scattering covering the kinematic domain 5 GeV$^2 \lesssim Q^2 \lesssim 100$ GeV^2 and $10^{-4} \lesssim x_{Bj} \lesssim 10^{-2}$. The analysis is based on data collected with the H1 detector at HERA in 1994 corresponding to an integrated luminosity of about 2 pb^{-1}. The results have been corrected for detector effects. Jets are defined using a cone type algorithm in the photon-proton center of mass system requiring jet transverse momenta of at least 5 GeV. Jet rates are shown as a function of Q^2 and x_{Bj}, and are compared to several QCD models. Leading order and next to leading order QCD calculations, assuming interactions of point-like virtual photons are not able to describe the data. A model based on point-like and resolved virtual photon structure gives a good description of the data as does a model based on gluon radiation from color dipoles.

Abstract 247
Parallel Sessions 2, 3, 4
Plenary Sessions 1, 3, 4

1 Introduction

The study of jets in deep inelastic lepton proton scattering (DIS) provides a testing ground for perturbative QCD. Partons emerging from the scattering process manifest themselves in jets which are observable in the experiment.

In lowest order, i.e. the quark parton model, the virtual photon is absorbed by a single quark (antiquark) of the proton resulting in one jet from the struck quark and one from the proton remnant. Both jets have small transverse momenta in the photon-proton center of mass frame (cms). To first order in the strong coupling constant α_s, two jets with balanced transverse momenta in the cms are produced either by gluon emission from the scattering quark ($\gamma q \to qg$) or by the photon gluon fusion process ($\gamma g \to q\bar{q}$).

The rate of dijet events is the basic observable for more sophisticated analyses, as the measurement of α_s [1] or the determination of the gluon density within the proton [2].

In this analysis we present a measurement of the dependence of the fraction R_2 of dijet events in all DIS events on the scaling variable x_{Bj}, integrated over Q^2, and on the virtuality of the exchanged photon Q^2, integrated over x_{Bj}. Jets are defined using a cone type algorithm in the photon-proton center of mass system requiring jet transverse momenta of at least 5 GeV. The measured jet rates are corrected for detector effects.

Previous measurements of jet production at HERA [3] used the JADE jet algorithm at large photon virtualities Q^2 and moderate jet transverse momenta p_T. This analysis probes a new region of jet phase space characterized by jet transverse momenta of similar size or larger than the photon virtuality, $p_T^2/Q^2 \gtrsim 1$. Moreover, the JADE algorithm restricts the phase space to high values (typically $\gtrsim 0.02$) of the fractional momentum of the parton entering the hard subprocess. The cone algorithm with a 5 GeV p_T threshold, on the other hand, is sensitive to fractional parton momenta down to 0.003.

The measurement has been performed with the H1 detector at the HERA storage ring, where 27.5 GeV positrons collide with 820 GeV protons.

2 QCD Calculation of Dijet Rates

Hard scattering processes are expected to be well described by perturbative QCD. In this analysis they are selected by asking for two jets with transverse momenta above 5 GeV. We consider four different QCD models labeled DIR, RES, CDM, and NLO. We briefly describe their most important features.

DIR: The QCD matrix elements in leading order in α_s (photon-gluon fusion and the QCD-Compton process) are convoluted with parton densities in the proton. Only "direct" (point-like) interactions of the photon are considered. For this model we have used the LEPTO [4] and RAPGAP [5] Monte Carlo (MC) programs.

RES: In addition to the point-like contribution discussed above, a contribution from quarks and gluons inside the photon is considered. For this model a parameterization of the virtual photon structure is needed. We use the SaSgam-2D parameterization [6] with the invariant mass squared of the hard subprocess $\hat{s}$ as scale. This model is implemented in the RAPGAP program.

In both the DIR and RES models additional emissions are generated by parton showers [7] in the leading log DGLAP [8] approximation. As a consequence the radiated partons are strongly ordered in transverse momentum k_t with the hardest emission in the ladder occuring next to the hard matrix element (Figs. 1a and 1b).

CDM: In the color dipole model [9], as implemented in ARIADNE [10], gluon emission originates from a color dipole stretched between the scattered quark and the proton remnant. Each emission of a gluon leads to two dipoles which may radiate further, leading to a cascade of independently radiating dipoles (Fig. 1c). These gluons are not ordered in k_t along the "ladder". The CDM description of gluon emission is similar to that of the BFKL [11] evolution, in which the gluons perform a random walk in k_T.

The dipole model has been very successful in describing the hadronic final state in e^+e^- annihilation. For DIS three additional features have been incorporated. The photon gluon fusion process, which is not naturally described by the CDM, is treated similarly as in the DIR approach discussed above. In this model, however, it constitutes only approximately one third of the dijet cross section in the phase space region considered in this analysis [12]. The color charge of the proton remnant (a diquark in the simplest case) is assumed not to be point-like leading to a phenomenological suppression of gluon radiation [10] in the direction of the remnant. The suppression sets in for hard gluons with wavelengths smaller than the size of the remnant. In addition, also the color charge of the scattered quark is taken to be spread out, depending on the virtuality Q^2 of the photon. This in turn leads to a suppression of radiation in the direction of the scattered quark [10].

In the DIR, RES, and CDM models hadronization was performed with the Lund string fragmentation scheme as implemented in JETSET [13].

NLO: Finally, we consider an exact calculation in next to leading order (NLO) in the strong coupling constant α_s as implemented in the Monte Carlo integration programs MEPJET [14] and DISENT [15]. They provide cross sections at the parton level rather than a full hadronic final state.

Unless stated otherwise, we use the GRV 94 HO parameterization [16] of parton densities inside the proton. We use a $\Lambda^{(4)}_{QCD}$ of 250 MeV. In the DIR, RES, and CDM models the one loop expression for the calculation of α_s was used. The NLO calculations by DISENT and MEPJET use the two loop expression.

3 The H1 Detector

A detailed description of the H1 apparatus is given elsewhere [17]. The parts of the detector which were essential for this measurement are the liquid argon calorimeter (LAr), the backward lead-scintillator calorimeter (BEMC) and the tracking chamber system.

The energy of the scattered positron is measured in the BEMC which has a depth of 21.7 radiation lengths and covers the Θ (the polar angle with respect to the proton beam direction) range from 151° to 176°. Its position is determined with the backward tracking system located in front of the BEMC covering $155.5^\circ < \Theta < 174.5^\circ$.

The hadronic energy flow is detected in the LAr which extends from $4^\circ < \Theta < 153^\circ$. The depth of the LAr varies between 4.5 and 8 hadronic interaction lengths.

Charged tracks in the central region ($25^\circ < \Theta < 155^\circ$) are measured in the central drift chamber system. The forward tracking detector covers $5^\circ < \Theta < 25^\circ$.

4 Data Selection

The data sample used for the present analysis corresponds to an integrated luminosity of 1.97 pb^{-1} taken during the 1994 run period. The phase space region of DIS events considered in this analysis is defined as follows:

$$\begin{aligned} 156^\circ < \quad \theta_e &\quad < 173^\circ \\ E' &\quad > 11\,\mathrm{GeV} \\ y &\quad > 0.05 \end{aligned} \tag{1}$$

Here, θ_e is the polar angle of the scattered positron and E' is its energy. The kinematic variables x_{Bj}, Q^2, and y are determined from the scattered positron. Additional cuts are applied to suppress the influence of QED radiation and photoproduction background, where the scattered positron is undetected in the backward direction, and a hadron entering the BEMC is misidentified as a positron.

5 Jet Reconstruction and Selection

Jets are reconstructed using clusters of energy measured in the LAr calorimeter. The corrected hadronic energy and the direction from the interaction point to the cluster center are used to construct a massless four-vector.

Due to noise limitations and dead material in front of the calorimeter the efficiency of the calorimeter to detect low energy particles is rather low. This can be improved by using in addition to the calorimeter information also charged tracks in the jet reconstruction. Charged tracks contribute at most 300 MeV of momentum. Below this limit the true track momentum is used. The value of 300 MeV was found to be optimal to reconstruct the jets' transverse momenta using simulated events.

Jets are defined in this analysis using a cone algorithm [18]. A jet is found in the hadronic cms[1] by maximizing the scalar sum of the transverse momenta p_t^* over a circular area of given radius R in the $\eta^* - \phi^*$ plane and requiring that it exceeds a minimum value $p_t^{*\min}$. Here η^* and ϕ^* are the pseudorapidity and azimuthal angle of the massless four-vectors in the hadronic cms. The η^* and ϕ^* of the resulting jet(s) are calculated as the p_t^*-weighted sums of η^* and ϕ^* of the massless calorimeter objects and tracks which are assigned to the jet(s). This recombination scheme is usually called the "p_t"-scheme.

In this analysis, the cone algorithm parameters

$$R = 1 \quad \text{and} \quad p_t^{*\min} = 5\,\mathrm{GeV} \tag{2}$$

have been chosen. Exactly two jets fulfilling this criterion are demanded. In addition the pseudorapidity difference $\Delta\eta^*$ of the two jets is required to be in the range

$$|\Delta\eta^*| < 2 \tag{3}$$

to suppress events with jets from parton showering and the proton remnant. This cut is equivalent to requiring $|\cos\hat{\theta}| < 0.76$, where $\hat{\theta}$ is the polar angle between the emerging and incoming partons in the gamma-parton center of mass frame.

To obtain the dijet rate R_2 the number of dijet events is compared to the total number of events in the same region of x_{Bj} and Q^2. R_2 is measured in bins of x_{Bj}, integrated over Q^2, and in bins of Q^2, integrated over x_{Bj}.

[1] Variables measured in the hadronic cms are marked by a *. The positive z direction is defined to be along the incident proton.

6 Corrections of Data

Residual background from photoproduction was statistically subtracted with the help of the PHOJET Monte Carlo generator [19]. This generator has been proven to give a reasonable description of photoproduction background in Ref. [20]. The subtraction for the total event sample amounts to 14% and 9% in the lowest x_{Bj} and Q^2 bins, respectively. It is below 5% in all other bins. The subtraction for the dijet sample is 3% or less. The resulting correction of the jet rate is only significant in the lowest x_{Bj} and Q^2 bins, where it raises the rate by about 10%.

The correction of data for detector acceptance and efficiencies is performed using two Monte Carlo models, LEPTO [4] and ARIADNE [10], with two sets of parton density parameterizations, MRS-H [21] and GRV 94 HO [16].

These models are used to obtain bin by bin correction factors $c = R_2^{MC,hadrons}/R_2^{MC,recon.}$ for the dijet rate R_2. This procedure is justified since the observables of the jet events, which are sensitive to detector effects, are reasonably well described by the Monte Carlo simulation. Critical observables in this sense are the energy flow within and around the jets and the η^* and p_t^* distribution of jets. Figure 2 shows a comparison of the experimental distributions with the two Monte Carlo models. Only the curves obtained with the MRS-H parton density are shown, the GRV 94 HO curves are very similar. There is good agreement between data and simulated events except for the η^* distribution of jets. The jet reconstruction efficiency depends on η^*. Thus, an additional correction was applied which is proportional to the difference of the mean values of η^* between experiment and simulation in each bin. This additional correction amounts to -10% for the lowest x and Q^2 bins and decreases to -1% with increasing x and Q^2.

Radiation of photons from the incoming or outgoing positron lead to measured values of x_{Bj}, Q^2, and y which differ from the ones effective in the hadronic interaction. This influences the values of R_2 due to the x_{Bj} and Q^2 dependence of R_2 and the y cut in the event selection. This was corrected for using the DJANGO Monte Carlo generator [22]. The correction factor was found to be $c_{\mathrm{rad}} = 1.08$, independent of x_{Bj} and Q^2.

The combined correction factors of all corrections discussed above vary between 1 and 1.2 for low and high x and Q^2 values, respectively.

7 Systematic Errors

Several sources of systematic uncertainties were investigated. A change in the hadronic energy scale of the LAr calorimeter by its estimated precision of $\pm 4\%$ results in a global change of jet rates by $^{+9\%}_{-7\%}$. The radiative correction has a global uncertainty of $\pm 3\%$ based on Monte Carlo statistics. These two errors were added in quadrature to give an overall systematic error.

Changing the energy scale of the positron measurement in the BEMC within its $\pm 1\%$ uncertainty results in a change of R_2 by $\pm 2\%$ in the Q^2 bins. In the x_{Bj} bins, the change varies between $\pm 1\%$ for the lowest and $\pm 9\%$ for the highest bin. The systematic errors on the corrections for acceptance and efficiency were obtained by using the maximal variation of the correction factor for any particular model compared to the mean in each bin. They are on the order of 10%. These two errors were added in quadrature to give a bin by bin systematic error.

8 Results and Discussion

Figures 3a and 3b show the fractional dijet rate in all DIS events as a function of Q^2 and x_{Bj} respectively. Data are corrected for detector effects to the hadron level. The correction has been performed to the phase space region defined by Eqs. 1 – 3. The data show a jet rate consistent with being flat in x_{Bj} and strongly rising in Q^2.

The results are compared to predictions of Monte Carlo models (c.f. section 2) based on perturbative QCD. The DIR model, implemented in the programs LEPTO and RAPGAP, fails to describe the data. Fig. 3 shows the RAPGAP result. In particular in the region of small Q^2 and x_{Bj} it undershoots data by a factor of more than three. RAPGAP and LEPTO give results consistent with each other within 10%. Varying the parton density parameterizations (GRV-LO, CTEQ-4HJ, MRS-H, MRS-R1) leads to variations of up to 30% in the lowest Q^2 and x_{Bj} bins and up 10% in the highest bins.

We conclude that a leading order matrix element calculation in combination with DGLAP parton showers as an approximation to higher order effects is not able to account for the observed jet rates. Therefore we now investigate if an exact next to leading order (NLO) calculation as implemented in the programs MEPJET [14] and DISENT [15] gives a better description of the data.

These programs provide parton level cross sections rather than a full hadronic final state. Therefore, Fig. 3 shows the parton level fractional dijet rate as given by a DISENT calculation compared to data at the hadron level. This comparison is justified by the fact that hadronization effects are small at jet transverse momenta above 5 GeV. Hadron level and parton level jet rates were compared using the DIR and CDM Monte Carlo models. They differ by not more than 20%.

Jet rates in NLO calculated with the program DISENT substantially exceed the DIR rates in the low Q^2 and x_{Bj} bins and approach the DIR rates in the high bins. Nevertheless, they too fall significantly below the data at all values of Q^2 and x_{Bj}. Varying the parameterization of parton densities in the proton (GRV-LO, CTEQ-4HJ, MRS-R1) changes the results by not more than 30% in the lowest Q^2 and x_{Bj} bin, and not more than 10% in the highest bins. The MEPJET program gives results consistent with DISENT within 2%. We conclude that replacing the parton shower approximation by an exact next to leading order calculation does not resolve the discrepancy with data.

The CDM model as implemented in ARIADNE gives a good description of the dijet rate, both in absolute height and in the Q^2 and x_{Bj} dependence. Note, however, that by tuning of model parameters (proton and photon size suppression) predictions of this model can be varied by up to 30%.

The RES model as implemented in RAPGAP is also able to give a good description of the data. Also here considerable freedom exists in tuning the model to data (parton densities in the virtual photon, choice of scale and starting scale for parton evolution in the virtual photon).

In the DGLAP picture, as implemented in the DIR model, the hardest emission always occurs at the photon vertex. Further parton emissions are strongly ordered with the transverse momentum k_T decreasing towards the proton. A common feature of the CDM and the RES model is the breaking of k_T ordering between the photon and the proton vertex. The hardest emission leading to the observed jets may occur anywhere in the ladder depicted in Fig. 1. In this case, additional hadronic activity is expected from the virtual photon "remnant" and possible additional parton emission from the top part of the ladder (Fig.1b). This activity is expected in the direction of the virtual photon, i.e. in the backward region of the detector. Both models predict a Q^2 dependence of this effect which increases as Q^2 approaches 0. These models may provide a smooth transition to photoproduction.

To make a qualitative argument we define an observable which is sensitive to additional energy flow in the photon direction (i.e. in the backward region of the detector):

$$x_\gamma = \frac{\Sigma_{jets}(E - p_z)}{\Sigma_{all}(E - p_z)} \tag{4}$$

In the limit $Q^2 \to 0$ this corresponds to the fractional momentum of the parton from the photon entering the hard subprocess giving rise to the observed jet system. In this picture $1 - x_\gamma$ corresponds to the fractional energy of the photon remnant.

Fig. 4a shows the uncorrected (i.e. detector level) distribution of x_γ in data for three different ranges in Q^2. An increase at low x_γ is observed as Q^2 decreases. No such effect is observed in the DIR model (Fig. 4b) while both the CDM model and a mixture of direct and resolved processes according to the RES model show a similar effect. This observation can be interpreted as an indication of the hardest emissions, leading to the observed jets, occuring away from the photon vertex.

9 Conclusions

Fractional dijet rates have been measured in deep inelastic scattering at small x_{Bj} (10^{-2} to 10^{-4}) and moderate Q^2 (5 GeV^2 to 100 GeV^2). Data have been corrected for detector effects.

This analysis probes a new region in jet phase space (small x_{Bj}, jet transverse momenta of similar size or larger than the photon virtuality, $p_T^2/Q^2 \gtrsim 1$).

QCD calculations in leading and next to leading order in α_s, assuming a point-like photon, fail to describe the data.

The data can be described by introducing an additional contribution from resolving partons inside the virtual photon. The color dipole model of gluon emission also gives a good description of the data. In both models the hardest emission, leading to the observed jets, is not bound to occur at the photon vertex. This leads to a breaking of ordering in transverse momentum k_T for parton emissions between the photon and the proton vertex.

Acknowledgements

We are grateful to the HERA machine group whose outstanding efforts have made and continue to make this experiment possible. We thank the engineers and technicians for their work in constructing and now maintaining the H1 detector, our funding agencies for financial support, the DESY technical staff for continual assistance, and the DESY directorate for the hospitality which they extend to the non-DESY members of the collaboration. We would like to thank L. Lönnblad und J. Rathsman for fruitful discussions.

References

[1] H1 Collaboration, T. Ahmed et al., Phys. Lett. B346 (1995) 415;
ZEUS Collaboration, M. Derrick et al., Phys. Lett. B363 (1995) 201.

[2] H1 Collaboration, T. Ahmed et al., Nucl. Phys. B449 (1995) 3.

[3] H1 Collaboration, I. Abt et al.,Z.Phys. C61 (1994) 59;
ZEUS Collaboration, M. Derrick et al., Z. Phys. C67 (1995) 81.

[4] G. Ingelman, in Proc. Workshop on Physics at HERA, Hamburg, October 1991, eds. W. Buchmüller and G. Ingelman, vol. 3, p. 1366 (1992).
We used the program versions 6.4 and 6.5.

[5] H. Jung, Comput. Phys. Commun. 86 (1995) 147.
We used the program version 2.06.

[6] G. Schuler and T. Sjöstrand, Z. Phys. C68 (1995) 607, Phys. Lett. B376 (1996) 193.

[7] M. Bengtsson, T.Sjöstrand, Z. Phys. C37 (1988) 465.

[8] V. N. Gribov and L. N. Lipatov, Sov. J. Nucl. Phys. 15 (1972) 438;
G. Altarelli and G. Parisi, Nucl. Phys. B126 (1977) 298;
Yu. L. Dokshitser, Sov. Phys. JETP 46 (1977) 641.

[9] G. Gustafson, Phys. Lett. B175 (1986) 453;
G. Gustafson, Ulf Petterson, Nucl. Phys. B306 (1988);
B. Andersson, G. Gustafson, L. Lönnblad, Ulf Petterson, Z. Phys. C43 (1989) 625.

[10] L. Lönnblad, Comput. Phys. Comm. 71 (1992) 15;
L. Lönnblad, Z. Phys. C65 (1995) 285.
We used the program version 4.08.

[11] E. A. Kuraev, L. N. Lipatov and V. S. Fadin, Sov. Phys. JETP 45 (1977) 199;
Ya. Ya. Balitsky and L. N. Lipatov, Sov. J. Nucl. Phys. 28 (1978) 822.

[12] J. Rathsman, Phys. Lett. B393 (1997) 181.

[13] T. Sjöstrand, Comp. Phys. Comm. 82 (1994) 74;
T. Sjöstrand, Pythia 5.7 and Jetset 7.4 physics and manual, CERN-TH 7112/93, Dec. 1993 (revised Aug. 1994).

[14] E. Mirkes and E. Zeppenfeld, Phys. Lett. B380 (1996) 105 [hep-ph/9511448].

[15] S. Catani and H. Seymour, Acta Phys. Polon. B28 (1997) 863.

[16] M. Glück, E. Reya, A. Vogt, Z. Phys. C67 (1995) 433.

[17] H1 Collaboration, I. Abt et al, *The H1 Detector at HERA*, Nucl. Instr. and Meth. A386 (1997) 310.

[18] M. H. Seymour Z. Phys. C62 (1994), 127.

[19] R. Engel et. al. Z. Phys. C 66 (1995) 203

[20] H1 Collaboration, S. Aid et al., Nucl. Phys. B470 (1996) 3.

[21] A.D. Martin, W.J. Stirling and R.G. Roberts, in Proc. Workshop on Quantum Field Theory and Theoretical Aspects of High Energy Physics, Bad Frankenhausen, Germany, 1993, eds. B. Geyer and E.M. Ilgenfritz (1993) p. 11.

[22] K. Charchula, G. Schuler, H. Spiesberger, Comput. Phys. Commun. 81 (1994) 381.
We used the program version 6.2.

[23] A. Kwiatkowski, H. Spiesberger and H.-J. Möhring, Comput. Phys. Comm. 69 (1992) 155.

Figures

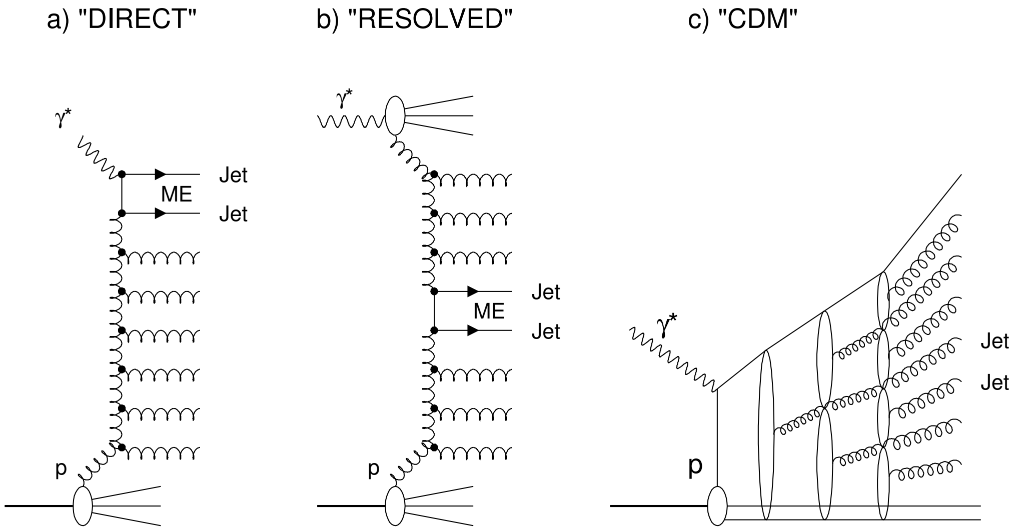

Figure 1: Generic diagram of parton emission in ep scattering (a,b). In the "direct" process (a) the hardest emission given by the QCD matrix element occurs at the top of the ladder. Emissions down the ladder are ordered with decreasing transverse momenta. In the "resolved" process (b) the hardest emission given by the QCD matrix element may occur anywhere in the ladder with increasingly softer emissions down the ladder towards the proton and the photon. In the color dipole model (c) gluon emissions are not ordered in transverse momentum.

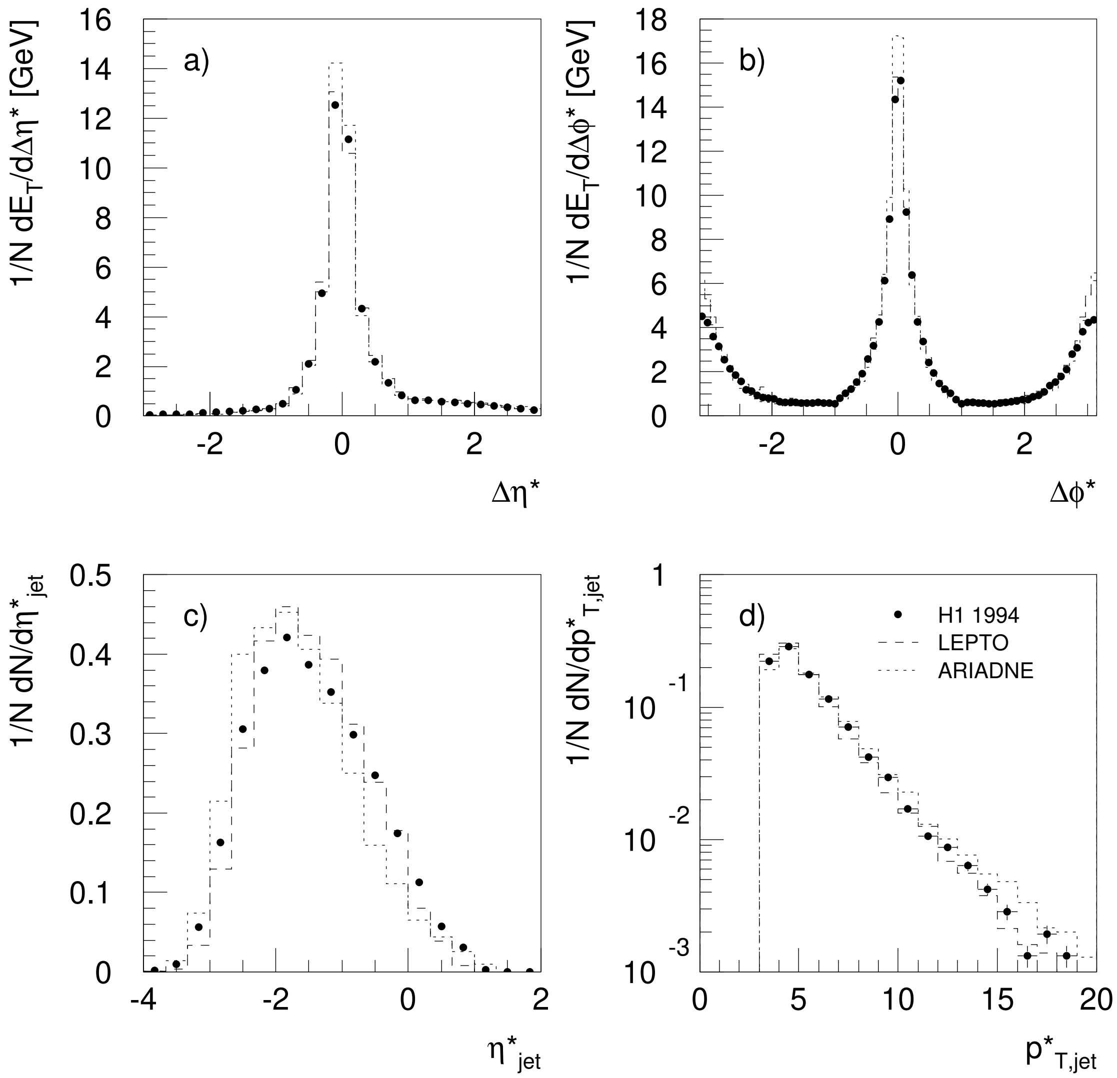

Figure 2: Transverse energy flow with respect to the jet axis, a) versus $\Delta\eta^*$ in a slice of $\Delta\phi^* < 1$, b) versus $\Delta\phi^*$ in a slice of $\Delta\eta^* < 1$. In the figures c) and d) the η^* and p_t^* spectra of the jets are shown. Points denote data, the histograms show the distributions obtained from LEPTO (dashed) and ARIADNE (dotted). The diagrams are normalized to the number N of jets; note that each dijet event counts twice.

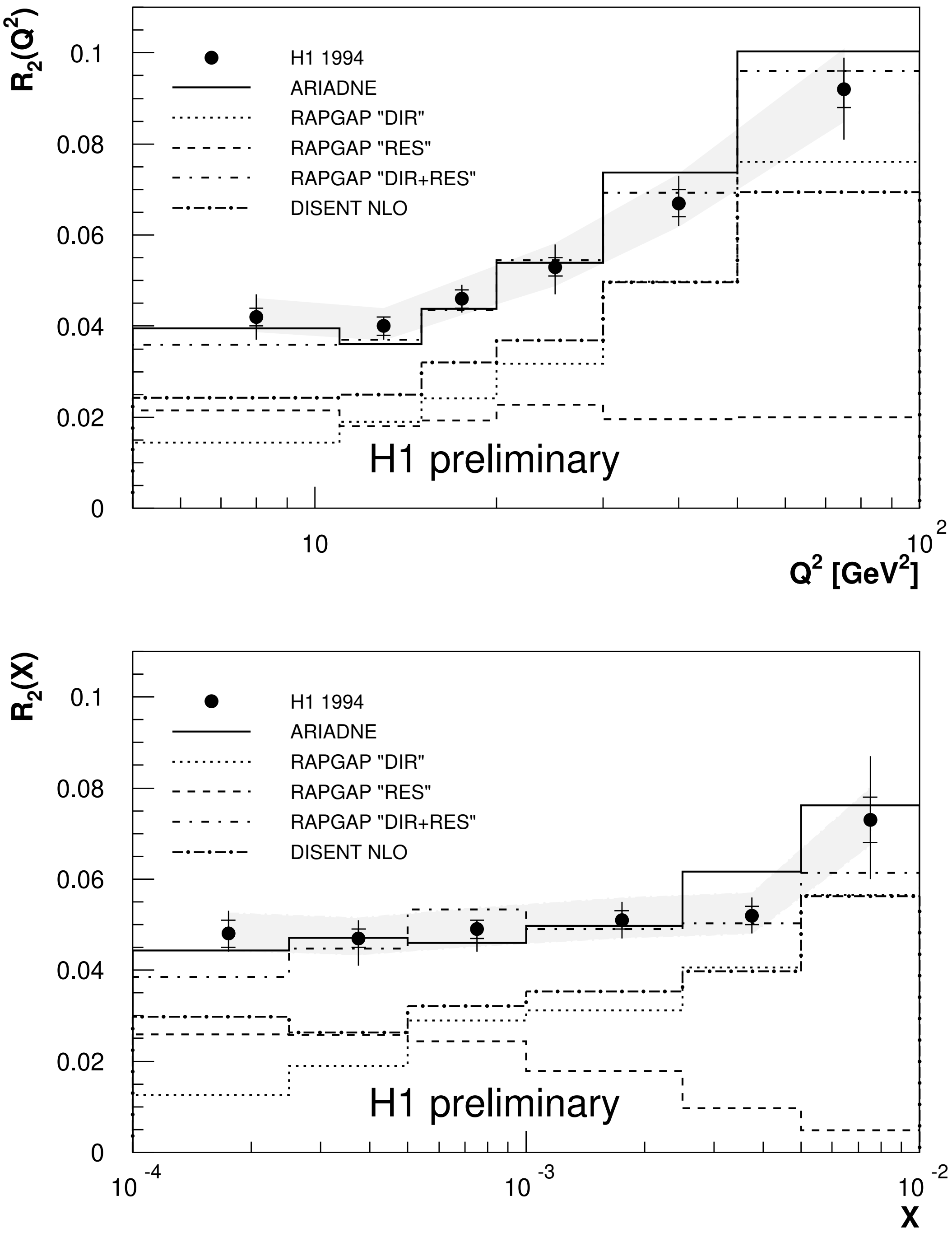

Figure 3: Fractional rate R_2 of dijet events as function of Q^2, integrated over x_{Bj} (a) and as a function of x_{Bj}, integrated over Q^2 (b). The inner bars give the statistical errors, the full error bars include the model dependence of the detector correction. The grey band shows the global uncertainty due to the hadronic energy scale of the calorimeter and the uncertainty of the radiative correction. Also indicated are the predictions of several QCD model calculations. Their statistical errors are of the same order as the statistical error of the data.

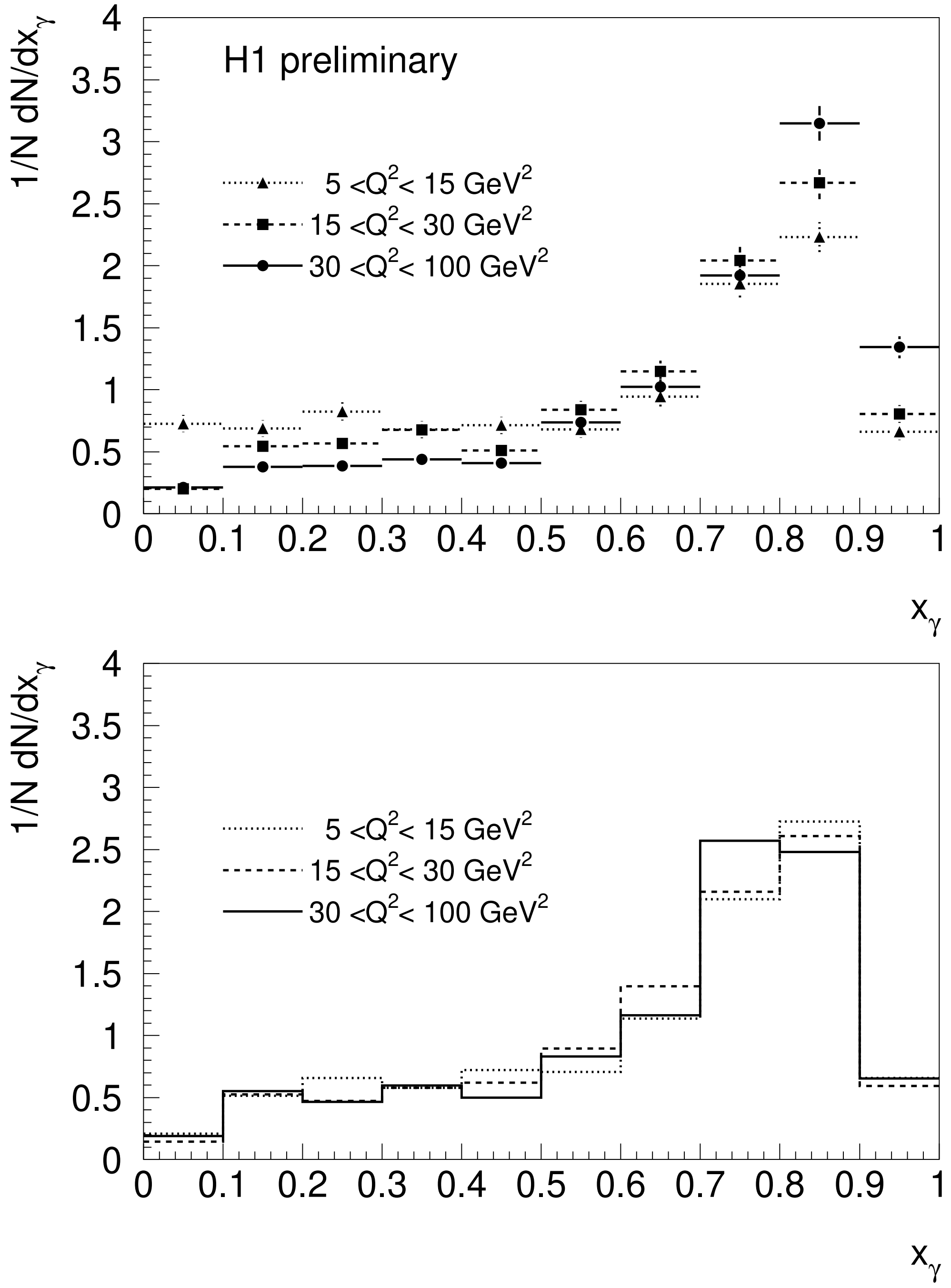

Figure 4: Distribution in the variable x_γ as defined in Eq. 4 for data (a) and for the LEPTO DIR model (b) (detector level). It is shown for three different ranges of photon virtuality Q^2. The figures are normalized to the number N of dijet events.